reviews

Determining the structures of large proteins and protein complexes by NMR

G. Marius Clore and Angela M. Gronenborn

Recent advances in multidimensional NMR methodology to obtain ^{1}H, ^{15}N and ^{13}C resonance assignments, interproton-distance and torsion-angle restraints, and restraints that characterize long-range order have, coupled with new methods of structure refinement, permitted solution structures of proteins in excess of 250 residues to be solved. These developments may permit the determination by NMR of the structures of macromolecules up to 50–60 kDa, thereby bringing into reach numerous systems of considerable biological interest, including a large variety of protein–protein and protein–nucleic-acid complexes.

It is axiomatic that a detailed understanding of the function of a macromolecule requires knowledge of its three-dimensional (3D) structure. At the present time, the two main techniques that can provide a complete description of the structure of macromolecules at the atomic level are X-ray crystallography, in the solid state (single crystals), and nuclear magnetic resonance (NMR) spectroscopy, in solution. The rate-limiting factors in solving an X-ray structure lie in obtaining not only suitable crystals that diffract to sufficient resolution but also appropriate heavy–atom derivatives to determine the phases of the reflections accurately. Despite significant advances in crystallization methods and the advent of new developments, such as multiple anomalous dispersion to facilitate phase determination, the number of X-ray protein structures solved to date is several orders of magnitude smaller than the number of available protein sequences. Unlike crystallography, NMR measurements are carried out in solution under potentially physiological conditions, and are therefore not hampered by the ability or inability of a protein to crystallize.

The size of macromolecular structures that can be solved by NMR has been dramatically increased over the past few years[1]. The development of a wide range of two-dimensional (2D) NMR experiments in the early 1980s culminated in the determination of the structures of a number of small proteins[2,3]. Under exceptional circumstances, 2D NMR techniques can be applied successfully to determine the structure of proteins of up to 100 residues[4,5]. Beyond 100 residues, however, 2D NMR methods fail, owing principally to spectral complexity that cannot be resolved in two dimensions. In the late 1980s and early 1990s, a series of major advances took place, in which the spectral resolution was increased by extending the dimensionality to three and four dimensions[1]. In addition, by combining such multidimensional experiments with heteronuclear NMR, problems associated with large line widths can be circumvented by making use of heteronuclear couplings that are large relative to the line widths. Concomitant with the spectroscopic advances, significant improvements have taken place in the accuracy with which macromolecular structures can be determined. Thus it is now possible to determine the structures of proteins in the 15–35 kDa range at a resolution comparable to 2.5-Å-resolution crystal structures. The upper limit of applicability is probably 60–70 kDa, and the largest single-chain proteins solved to date are around 30 kDa, comprising some 260 residues[6,7]. Key improvements for increasing the accuracy of NMR structures include direct refinement against accurate coupling constants[8] and ^{13}C and ^{1}H shifts[9,10], as well as the use of conformational database potentials[11,12]. More recently, new methods have been developed to obtain structural restraints that characterize long-range order *a priori*[13,14]. These include making use of the dependence of heteronuclear relaxation on the rotational–diffusion anisotropy of nonspherical molecules, and of the field dependence of one-bond heteronuclear couplings arising from magnetic-susceptibility anisotropy. In this article, we summarize some of the recent developments in multidimensional NMR of biological macromolecules.

G. M. Clore and A. M. Gronenborn are at the Laboratory of Chemical Physics, National Institute of Diabetes and Digestive and Kidney Diseases, National Institutes of Health, Bethesda, MD 20892-0520, USA.

reviews

Basic principles of multidimensional NMR

An NMR spectrometer consists of two components: a high–field–strength superconducting magnet, in which the sample is located, and a console that can generate radio-frequency pulses in any desired combination.

Every proton possesses a property known as magnetization, and when a sample is placed in a static magnetic field B_0, the magnetization lies parallel to B_0 (defined as the z direction). To record a conventional one-dimensional NMR spectrum, a radio-frequency pulse B_1 is applied, which rotates the magnetization away from the z-axis towards the x–y plane. A free-induction decay is recorded immediately after the pulse, and Fourier transformation of this free–induction decay yields the conventional one-dimensional spectrum. To obtain additional information on interactions between spins, double or multiple irradiation experiments must be carried out. This requires the use of a second selective radiofrequency pulse B_2 at the position of a particular resonance. As long as there is no resonance overlap, the application of such experiments is relatively simple, but in the case of macromolecules, and proteins in particular, there is extensive spectral overlap, rendering this approach unfeasible.

The limitations of one-dimensional (1D) NMR can be overcome by extending the measurements into a second dimension. All 2D–NMR experiments use the same basic scheme[15], consisting of a preparation period, an evolution period (t_1) (during which the spins are labelled according to their chemical shift), a mixing period (during which the spins are correlated with each other), and finally a detection period (t_2). A number of experiments are recorded with successively incremented values of the evolution period t_1 to generate a data matrix, $s(t_1,t_2)$. 2D Fourier transformation of $s(t_1,t_2)$ then yields the desired 2D frequency spectrum $S(\omega_1,\omega_2)$. In most homonuclear 2D experiments, the diagonal corresponds to the 1D spectrum, and the symmetrically placed cross peaks on either side of the diagonal indicate the existence of an interaction between two spins. The nature of the interaction depends on the type of experiment. Thus, in a correlation (COSY) experiment, the cross peaks arise from through-bond scalar correlations, while in a nuclear Overhauser enhancement (NOE) experiment, they arise from through–space correlations.

The extension from 2D to 3D and 4D NMR is straightforward and illustrated schematically in Fig. 1[16]. Thus, a 3D experiment is constructed from two 2D experiments by leaving out the detection period of the first 2D experiment and the preparation pulse of the second. This results in a pulse train comprising two independently incremented evolution periods t_1 and t_2, two corresponding mixing periods M_1 and M_2, and a detection period t_3. Similarly, a 4D experiment is obtained by combining three 2D experiments in an analogous fashion. The real challenge of 3D and 4D NMR is twofold: first, to ascertain which 2D experiments should be combined to best advantage; and second, to design the pulse sequences in such a way that undesired artifacts, which may severely
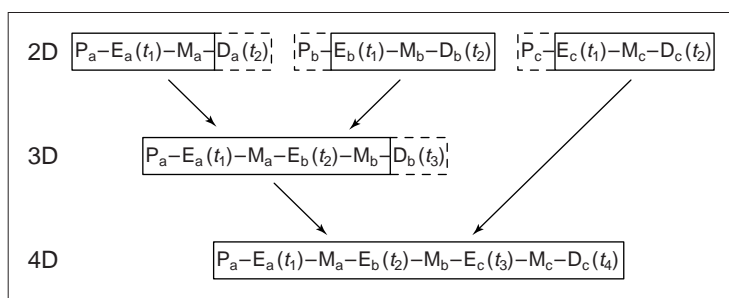
Figure 1

General representation of pulse sequences used in multidimensional nuclear magnetic resonance (NMR), illustrating the relationship between the basic elements used to record 2D, 3D and 4D NMR spectra. Note how 3D and 4D experiments are constructed by the appropriate linear combination of 2D experiments. Abbreviations: P, preparation; E, evolution; M, mixing; D, detection. In 3D and 4D NMR, the evolution periods are incremented independently. Reproduced from Ref. 1.

interfere with the interpretation of the spectra, are removed.

The nuclear Overhauser effect

The main source of geometric information used in protein-structure determination lies in the nuclear Overhauser effect, which can be used to identify protons separated by less than 5 Å. This distance limit arises from the fact that the NOE (at short mixing times) is proportional to the inverse-sixth power of the distance between the protons. Hence the NOE intensity falls off very rapidly with increasing distance between proton pairs. Despite the short-range nature of the observed interactions, the short approximate interproton-distance restraints derived from NOE measurements can be highly conformationally restrictive, particularly when they involve residues that are far apart in the sequence.

The principle of the NOE is relatively simple. Consider a simple system with only two protons, between which magnetization is exchanged by a process known as cross relaxation. Because the cross-relaxation rates in both directions are equal, the magnetization of the two protons at equilibrium is equal. The approximate chemical analogy of such a system would be one with two interconverting species with an equilibrium constant of 1. The cross-relaxation rate is proportional to two variables: r^{-6}, where r is the distance between the two protons; and τ_{eff}, the effective correlation time of the interproton vector. It follows that, if the magnetization of one of the spins is perturbed, the magnetization of the second spin will change. In the case of macromolecules, the cross-relaxation rates are positive and the leakage rate from the system is very small; this means that, at a long time following the perturbation event, the magnetization of the two protons would be equalized. The change in magnetization of proton i upon perturbation of the magnetization of proton j is known as the nuclear Overhauser effect. The initial build–up rate of the NOE is equal to the cross-relaxation rate, and hence proportional to r^{-6}.

In 1D NMR, the NOE can be observed in a number of ways, all of which involve the application of a

selective radio-frequency pulse at the position of one of the resonances. The simplest experiment involves the irradiation of resonance i for a time t, followed by acquisition of the spectrum. If proton j is close in space to proton i, its magnetization will be reduced, and this is best observed in a difference spectrum – subtracting a spectrum without irradiation from one with selective irradiation. An alternative approach involves the selective inversion of resonance i followed by acquisition after a time t. This particular experiment is the 1D analogue of the 2D experiment. In the 2D experiment, cross peaks between proton resonances i and j are observed when the two protons are close in space, and thus exchange magnetization via cross-relaxation.
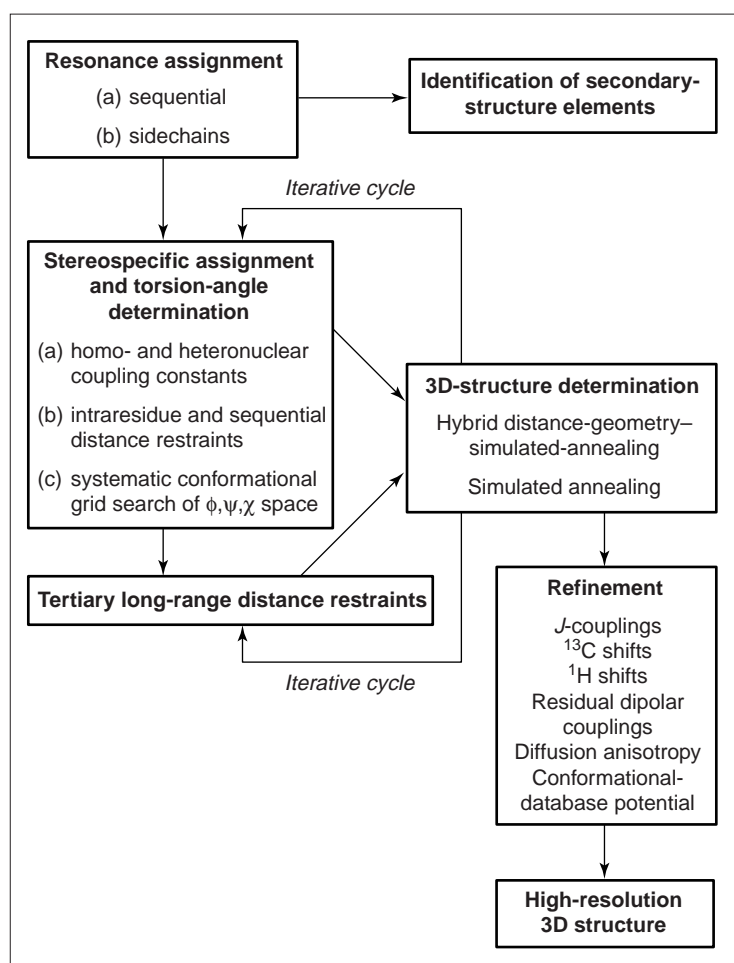
Figure 2

Summary of the general strategy employed to solve the three-dimensional structures of macromolecules by nuclear magnetic resonance. Hybrid distance-geometry–simulated-annealing involves initially generating an approximate polypeptide fold by projection of a subset of atoms from n-dimensional distance space into Cartesian-coordinate space, followed by simulated annealing that includes all atoms. Simulated annealing can also be carried out starting from either random structures with intact covalent geometry or from a completely random array of atoms. All simulated-annealing protocols involve solving Newton's equations of motion, subject to a target function that comprises terms for the experimental restraints, covalent geometry and nonbonded contacts. The basis of simulated annealing involves the use of initial high temperatures followed by slow cooling to overcome energy barriers along the path to the global minimum region of the target function.

General strategy for determining the structures of proteins and protein complexes by NMR

The power of NMR over other spectroscopic techniques results from the fact that every proton gives rise to an individual resonance in the spectrum that can be resolved by higher-dimensional (i.e. 2D, 3D and 4D) techniques. Bearing this in mind, the principles of structure determination by NMR can be summarized by the scheme depicted in Fig. 2. The first step is to obtain sequential resonance assignments using a combination of through-bond and through-space correlations; the second is to obtain stereospecific assignments at chiral centers, and torsion-angle restraints using three-bond scalar couplings combined with intraresidue and sequential-interresidue NOE data; the third step is to identify through-space connectivities between protons separated by less than 5 Å; the fourth and final step involves calculating 3D structures on the basis of the experimental NMR restraints, using one or more of a number of algorithms such as distance geometry and/or simulated annealing[17]. It is not essential to assign all the NOEs initially. Indeed, many may be ambiguous and several possibilities may exist for their assignments. In such cases, the NOE restraints can be dealt with as an ambiguous $(\Sigma r^{-6})^{-1/6}$ sum restraint, such that the restraint is satisfied providing only that at least one of the potential proton pairs is close. Once a low-resolution structure has been calculated from a subset of the NOE data that can be interpreted unambiguously, it is then possible to employ iterative methods to resolve the vast majority of ambiguities. Consider, for example, an NOE cross peak that could be attributed to a through-space interaction between either protons A and B or protons A and C; once a low-resolution structure is available, it is usually possible to discriminate between these two possibilities. If protons A and C are significantly greater than 5 Å apart while protons A and B are less than 5 Å apart, it is clear that the cross peak must arise from an NOE between protons A and B.

Sample requirements for NMR spectroscopy

In the study of macromolecules, concentrations of about 1 mM are typically employed, with a sample volume of 0.3–0.5 ml. A key requirement is that the macromolecule under study should be soluble, should not aggregate and should be stable for many weeks at room temperature. For ^{1}H-homonuclear work, it is also important to ensure that the buffer employed does not contain any protons. In general, two samples are required – one in D_2O, for the observation of nonexchangeable protons only, and the other in 95% H_2O / 5% D_2O, to permit the observation of exchangeable protons.

Although it is possible to use ^{1}H-homonuclear methods to solve the structures of proteins up to about 100 residues in certain, very favourable, cases[4,5], it is generally the case that extensive resonance overlap makes this task very time consuming and complex. Hence, providing that a protein can be overexpressed in a bacterial system, it is now desirable, even for proteins as small as 30 residues, to make use of the full

reviews
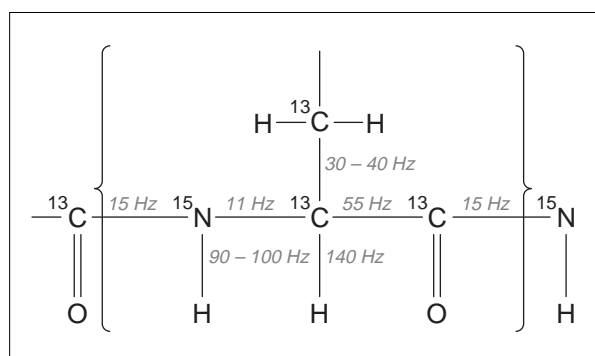
Figure 3
Summary of the one-bond heteronuclear couplings along the polypeptide chain utilized in 3D and 4D NMR experiments. Reproduced from Ref. 1.

panoply of multidimensional heteronuclear NMR experiments[1,18,19]. This makes the use of uniform ^{15}N- and ^{13}C-labelling necessary, which can be achieved by growing the bacteria on minimal medium containing $^{15}NH_4Cl$ and $^{13}C_6$-glucose as the sole nitrogen and carbon sources, respectively. In general, the following samples are required: ^{15}N-labelled sample in 95% H_2O/ 5% D_2O; ^{15}N- and ^{13}C-labelled sample in 95% H_2O/ 5% D_2O; and ^{15}N- and ^{13}C-labelled sample in D_2O. For very large systems, deuteration and specific labelling is advantageous[6,20,21]. For example, a particularly useful strategy for aromatic residues is reverse labelling, in which the aromatics are at natural isotopic abundance, while the other residues are ^{13}C- and ^{15}N-labelled[22]. This can be achieved by adding the aromatic amino acids at natural isotopic abundance to the minimal medium in addition to $^{15}NH_4Cl$ and $^{13}C_6$-glucose. A similar approach can also be used for various aliphatic amino acids. Deuteration of non-exchangeable protons is achieved by growing the bacteria in D_2O, rather than H_2O, medium.

Sequential assignment

Conventional sequential resonance assignment relies on 2D homonuclear ^1H–^1H correlation experiments to identify amino acid spin systems, and 2D ^1H–^1H NOE experiments to identify sequential connectivities along the backbone of the type $C^\alpha H(i)$–$NH(i + 1,2,3,4)$, $NH(i)$–$NH(i \pm 1)$ and $C^\alpha H(i)$–$C^\beta H(i + 3)$[2,3]. This methodology has been successfully applied to proteins of less than 100 residues, albeit with considerable effort[4,5]. For larger proteins, the spectral complexity is such that 2D experiments no longer suffice and it is essential to increase the spectral resolution by increasing the dimensionality of the spectra[1,16]. In some cases, it is still possible to apply the same sequential-assignment strategy by making use of 3D heteronuclear (^{15}N or ^{13}C) separated experiments to increase the spectral resolution[23]. Frequently, however, numerous ambiguities still remain and it is advisable to adopt a sequential-assignment strategy based solely on well-defined heteronuclear scalar couplings along the polypeptide chain[1,18,19], as shown in Fig. 3. The double- and triple-resonance experiments that we currently

use, together with the correlations that they demonstrate, are summarized in Table 1.

With the advent of pulsed-field gradients to either eliminate undesired coherence-transfer pathways[24] or enable the selection of particular coherence pathways coupled with sensitivity enhancement[25], it is now possible to employ only two- to four-step phase cycles without any loss in sensitivity (other than that due to the reduction in measurement time), such that each 3D experiment can be recorded in as little as 7 h. In most cases, however, signal-to-noise requirements require 1–3 days measuring time, depending on the experiment. For proteins greater than about 25 kDa, the assignment of the backbone and sidechain carbons is facilitated by making use of a sample in which the nonexchangeable protons are deuterated, thereby dramatically reducing the line widths[6]. Thus, for example, in the case of the 30 kDa N-terminal domain of Enzyme I (EIN), the average transverse relaxation time, T_2, for the backbone amides is increased from ~13 ms in the protonated sample to ~28 ms in the perdeuterated (that is, with the nonexchangeable protons replaced by deuterons) sample[6]. The resulting

Table 1. Summary of correlations observed in the three-dimensional double- and triple-resonance experiments used for sequential and sidechain assignments

Experiment name	Correlation	J coupling[a]
^{15}N-edited HOHAHA	$C^\alpha H(i)$–$^{15}N(i)$–$NH(i)$	$^3J_{HN\alpha}$
	$C^\beta H(i)$–$^{15}N(i)$–$NH(i)$	$^3J_{HN\alpha}$ and $^3J_{\alpha\beta}$
HNHA	$C^\alpha H(i)$–$^{15}N(i)$–$NH(i)$	$^3J_{HN\alpha}$
H(CA)NH	$C^\alpha H(i)$–$^{15}N(i)$–$NH(i)$	$^1J_{NC\alpha}$
	$C^\alpha H(i-1)$–$^{15}N(i)$–$NH(i)$	$^2J_{NC\alpha}$
HNCA	$^{13}C^\alpha(i)$–$^{15}N(i)$–$NH(i)$	$^1J_{NC\alpha}$
	$^{13}C^\alpha(i-1)$–$^{15}N(i)$–$NH(i)$	$^2J_{NC\alpha}$
HN(CO)CA	$^{13}C^\alpha(i-1)$–$^{15}N(i)$–$NH(i)$	$^1J_{NCO}$ and $^1J_{C\alpha CO}$
HNCO	$^{13}CO(i-1)$–$^{15}N(i)$–$NH(i)$	$^1J_{NCO}$
HCACO	$C^\alpha H(i)$–$^{13}C^\alpha(i)$–$^{13}CO(i)$	$^1J_{C\alpha CO}$
HCA(CO)N	$C^\alpha H(i)$–$^{13}C^\alpha(i)$–$^{15}N(i+1)$	$^1J_{C\alpha CO}$ and $^1J_{NCO}$
CBCA(CO)NH	$^{13}C^\beta(i-1)/^{13}C^\alpha(i-1)$–$^{15}N(i)$–$NH(i)$	$^1J_{C\alpha CO}$, $^1J_{NCO}$ and $^1J_{CC}$
CBCANH	$^{13}C^\beta(i)/^{13}C^\alpha(i)$–$^{15}N(i)$–$NH(i)$	$^1J_{NC\alpha}$ and $^1J_{CC}$
	$^{13}C^\beta(i-1)/^{13}C^\alpha(i-1)$–$^{15}N(i)$–$NH(i)$	$^2J_{NC\alpha}$ and $^1J_{CC}$
HBHA(CO)NH	$C^\beta H(i-1)/C^\alpha H(i-1)$–$^{15}N(i)$–$NH(i)$	$^1J_{C\alpha CO}$, $^1J_{NCO}$ and $^1J_{CC}$
HBHANH	$C^\beta H(i)/C^\alpha H(i)$–$^{15}N(i)$–$NH(i)$	$^1J_{NC\alpha}$ and $^1J_{CC}$
	$C^\beta H(i-1)/C^\alpha H(i-1)$–$^{15}N(i)$–$NH(i)$	$^2J_{NC\alpha}$ and $^1J_{CC}$
C(CO)NH	$^{13}Cj(i-1)$–$^{15}N(i)$–$NH(i)$	$^1J_{C\alpha CO}$, $^1J_{NCO}$ and $^1J_{CC}$
H(CCO)NH	$Hj(i-1)$–$^{15}N(i)$–$NH(i)$	$^1J_{C\alpha CO}$, $^1J_{NCO}$ and $^1J_{CC}$
HC–CH COSY	Hj–^{13}Cj–$^{13}Cj\pm1$–$Hj\pm1$	$^1J_{CC}$
HC–CH TOCSY	Hj–$^{13}Cj...^{13}Cj\pm n$–$Hj\pm n$	$^1J_{CC}$
HC–CH NOE	Hj–^{13}Cj–$^{13}Cj\pm1$–$Hj\pm1$	^{13}C–^{13}C NOE

[a] $^1J_{xy}$, $^2J_{xy}$ and $^3J_{xy}$ refer to couplings between atoms (x and y) separated by one, two and three bonds, respectively. In addition to the couplings indicated, all the experiments make use of the $^1J_{CH}$ (~140 Hz) and/or $^1J_{NH}$ (~95 Hz) couplings. The values of the couplings employed are as follows: $^3J_{HN\alpha}$, 3–10 Hz; $^1J_{CC}$, 35 Hz; $^1J_{C\alpha CO}$, 55 Hz; $^1J_{NCO}$, 15 Hz; $^1J_{NC\alpha}$, 11 Hz; $^2J_{NC\alpha}$, 7 Hz. With the exception of the HC–HC NOE experiment, the correlations observed in all the experiments occur via scalar couplings. In the case of the HC–HC NOE experiment, the correlation observed occurs via a through-space ^{13}C–^{13}C NOE.
Symbol: i, residue position along the polypeptide chain; j, carbon position within a given residue.

spectral improvement is readily ascertained from a comparison of the 2D ^{1}H–^{15}N correlation spectra of protonated and perdeuterated EIN (Fig. 4). The dramatic improvements attainable for EIN by deuteration in 3D triple-resonance NMR experiments is illustrated in Fig. 5.

Stereospecific assignments and torsion-angle restraints

Torsion-angle restraints can be derived from scalar-coupling-constant (J) data because simple geometric relationships exist between three-bond J couplings and torsion angles. In simple systems, the coupling constant can be measured directly from the in-phase or antiphase splitting of a particular resonance in the 1D or 2D spectrum. For larger systems, where the line widths exceed the coupling, it becomes difficult to extract accurate couplings in this manner. An alternative approach involves the use of ECOSY experiments to generate reduced cross-peak multiplets[26]. (In an ECOSY experiment, the coherence transfer observed in a regular 2D correlation COSY experiment is forced to take place exclusively between connected transitions in the energy-level diagram, thereby simplifying the fine structure of the cross-peak multiplets and permitting the various couplings to be measured readily.) Although this permits accurate couplings to

be obtained, the sensitivity of ECOSY experiments is generally quite low. Furthermore, in multidimensional experiments, its utility is restricted by the fact that the couplings have to be measured in the indirectly detected dimensions, and hence are influenced by limited digital resolution. More recently, a series of highly sensitive quantitative J-correlation experiments have been developed that circumvent these problems[27]. These experiments quantitate the loss in magnetization when the dephasing caused by coupling is active rather than inactive. In some quantitative J-correlation experiments, the coupling is obtained from the ratio of cross-peak to diagonal-peak intensities; in others, it is obtained from the ratio of the cross peaks obtained in two separate experiments (with the coupling active and inactive).

For small proteins, it is often possible to obtain stereospecific assignments of β-methylene protons on the basis of a qualitative interpretation of the homonuclear $^3J_{\alpha\beta}$ coupling constants and the intraresidue NOE data involving the NH, C$^\alpha$H and C$^\beta$H protons[28]. A more rigorous approach, which also permits the backbone ϕ (C$_{i-1}$–N$_i$–Cα_i–C$_i$) and ψ (N$_i$–Cα_i–C$_i$–N$_{i+1}$) and sidechain χ_1 (N–Cα–Cβ–Cγ/Oγ/Sγ) torsion-angle restraints to be obtained, involves the application of a conformational grid search of ϕ,ψ,χ_1 space on the basis of the homonuclear $^3J_{HN\alpha}$ and $^3J_{\alpha\beta}$ coupling
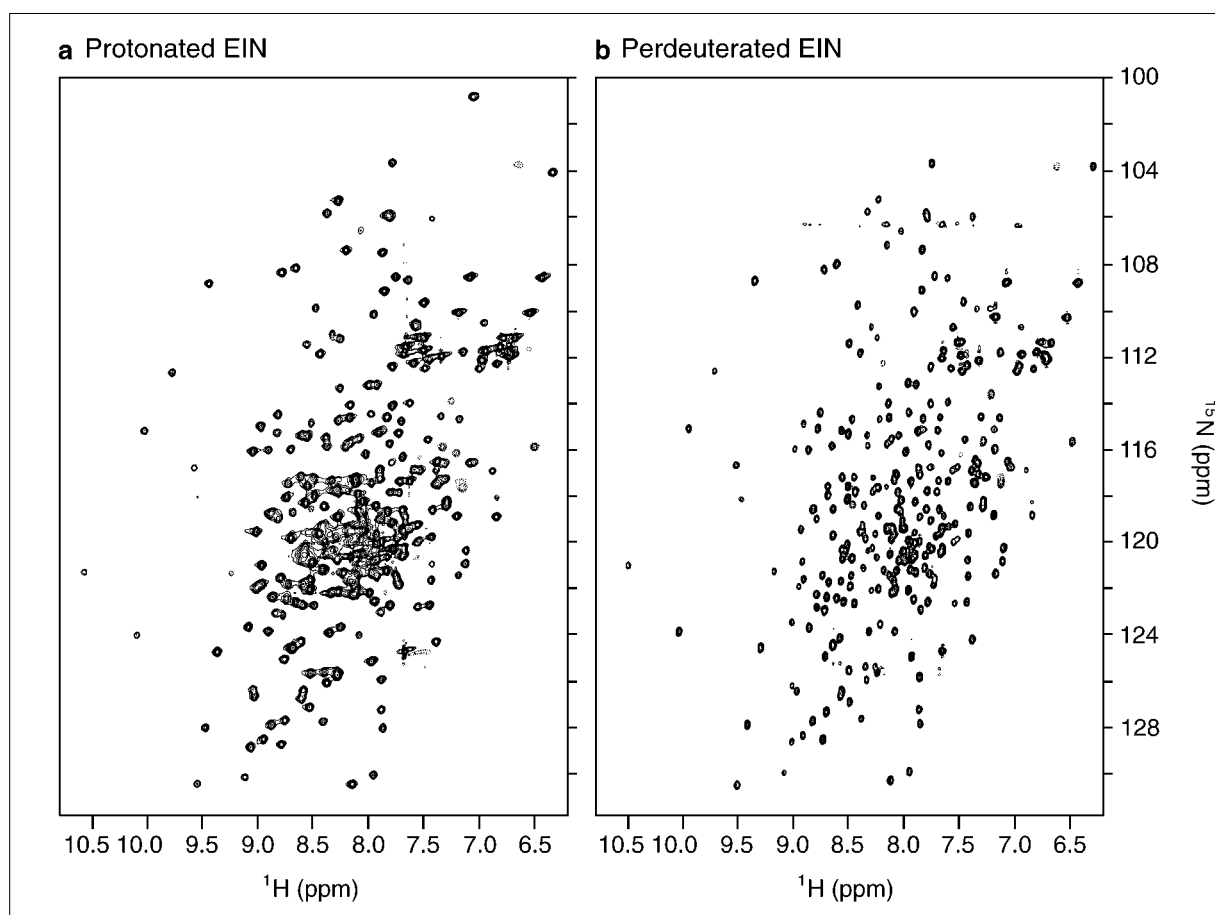
Figure 4

Comparison of the ^{1}H–^{15}N heteronuclear single-quantum-coherence (HSQC) spectrum of the protonated and perdeuterated ^{15}N-labelled N-terminal domain of Enzyme I. Reproduced from Ref. 6.
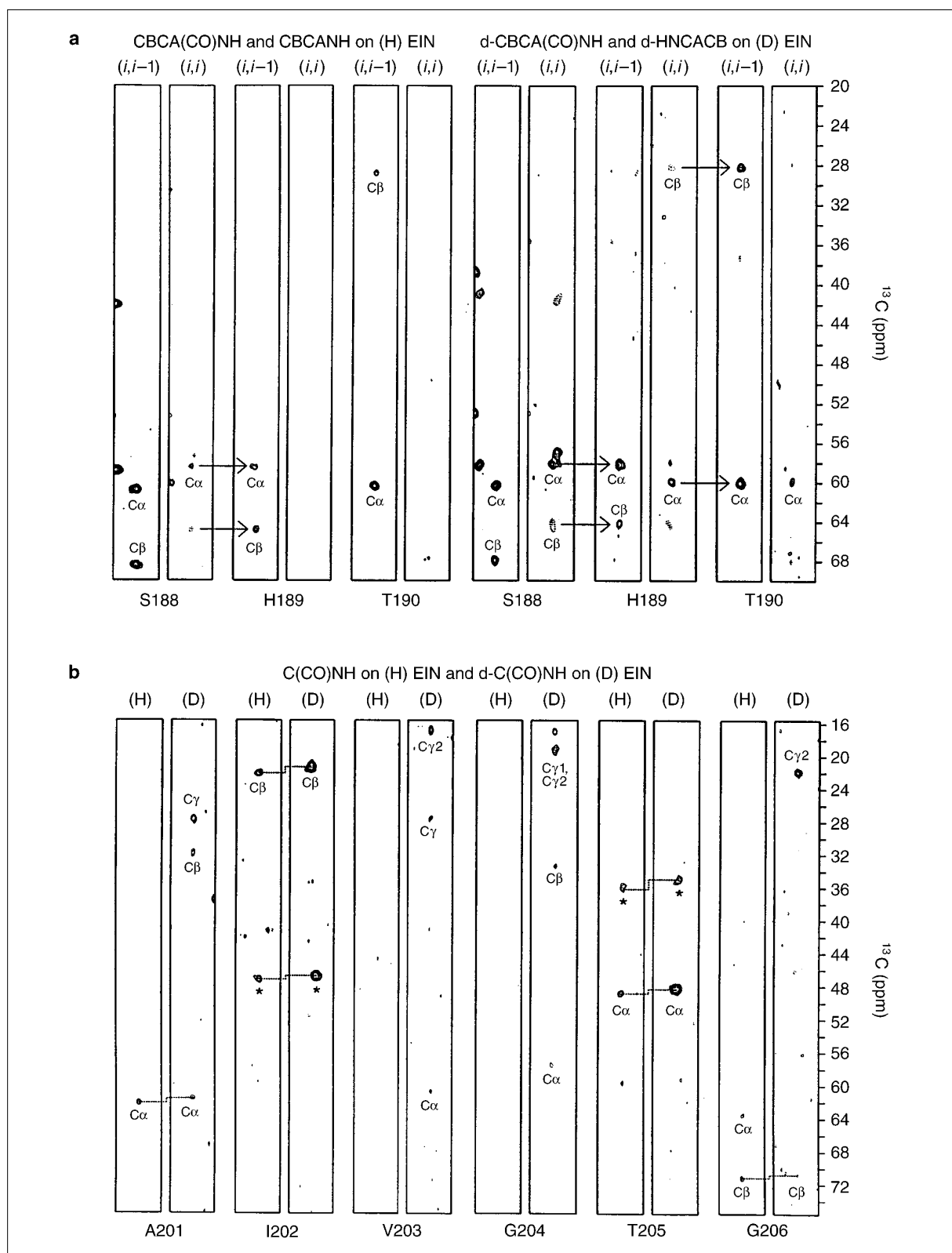
Figure 5

Selected strips taken from several 3D triple-resonance experiments, comparing the results on uniformly protonated and perdeuterated, uniformly ^{15}N–^{13}C-labelled N-terminal domain of Enzyme I. (**a**) CBCANH and CBCA(CO)NH experiments on protonated EIN [(H) EIN] versus the d-HNCACB and d-CBCA(CO)NH experiments on perdeuterated EIN [(D) EIN]. (**b**) C(CO)NH and d-C(CO)NH experiments on protonated and perdeuterated EIN, respectively (peaks labelled with an asterisk arise from resonances that have their maximal intensities on an adjacent slice). The CBCANH and d-HNCACB experiments correlate the Cα and Cβ resonances of both the (*i*–1) and *i* residues with the ^{15}N and ^1H resonances of residue *i*. The CBCA(CO)NH and d-CBCA(CO)NH experiments correlate only the Cα/Cβ resonances of the (*i*–1) residue with the ^{15}N and ^1H_N resonances of residue *i*. The C(CO)NH and d-C(CO)NH experiments correlate the sidechain and Cα resonances of residue (*i*–1) with the ^{15}N and ^1H_N resonances of residue *i*. Reproduced from Ref. 6.

reviews

Table 2. Experiments for determining three-bond (^3J) coupling constants by quantitative *J*-correlation spectroscopy

| Experiment	Ref.	Three-bond (^3J) coupling	Torsion angle
3D HNHA	27	$^3J_{HN\alpha}$	ϕ
3D (HN)CO(CO)NH	42	$^3J_{COCO}$	ϕ
2D ^{13}C–{^{15}N}-spin-echo difference CT-HSQC	27	$^3J_{C\gamma N}$	χ_1 of Thr and Val
2D ^{13}C–{^{13}CO}-spin-echo difference CT-HSQC	27	$^3J_{C\gamma CO}$	χ_1 of Thr and Val
2D ^{13}CO–{^{13}Cγ(aromatic)} spin-echo difference ^{1}H–^{15}N HSQC	45	$^3J_{C\gamma(aromatic)CO}$	χ_1 of aromatics
2D ^{15}N–{^{13}Cγ(aromatic)} spin-echo difference ^{1}H–^{15}N HSQC	45	$^3J_{C\gamma(aromatic)N}$	χ_1 of aromatics
2D ^{15}N–{^{13}Cγ} spin-echo difference ^{1}H–^{15}N HSQC	46	$^3J_{C\gamma(aliphatic)N}$	χ_1 of aliphatics
3D HN(CO)C	43	$^3J_{C\gamma(aliphatic)CO}$	χ_1 of aliphatics
3D HN(CO)HB	27	$^3J_{COH\beta}$	χ_1
3D HNHB	27	$^3J_{NH\beta}$	χ_1
3D HACAHB	44	$^3J_{\alpha\beta}$	χ_1
2D or 3D ^{1}H-detected long-range C–C COSY	27	$^3J_{CC}$	χ_2 of Leu and Ile χ_3 of Met
3D ^{1}H-detected (^{13}C–^{1}H) long-range COSY	27	$^3J_{CH}$	χ_2 of Leu and Ile χ_3 of Met
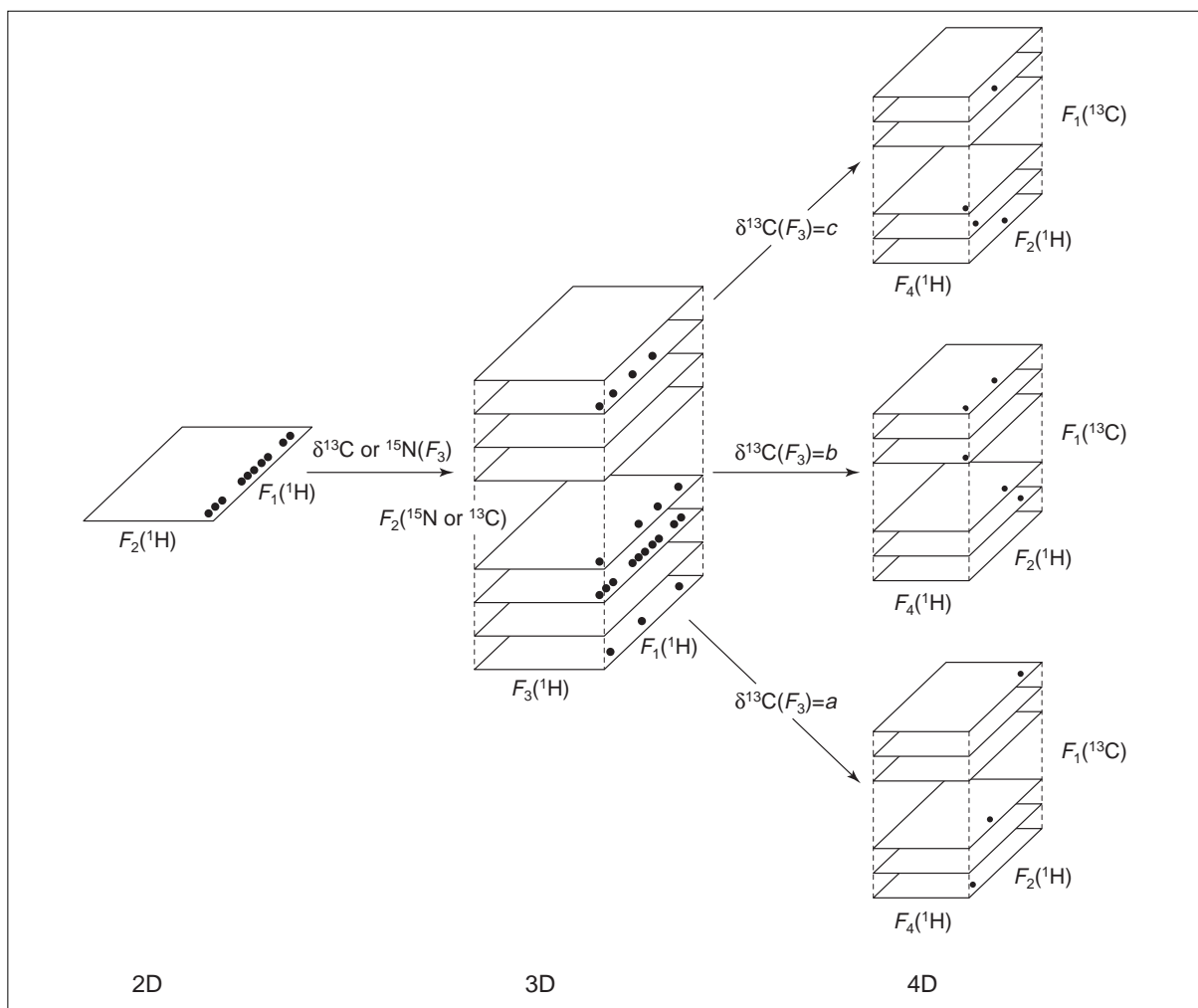
Figure 6

Schematic diagram illustrating the effects of increasing dimensionality on the spectral resolution of an NOE spectrum. In the 2D spectrum, the proton-chemical shift of the destination resonances (along the F_2 axis) for all 11 cross peaks is the same, so the number of destination protons involved cannot be assessed. In the 3D spectrum, the cross peaks appear in three planes, separated according to the shift of the heavy atom (^{15}N or ^{13}C) attached to the destination protons. The identity of the originating protons, however, is only defined by their proton-chemical shifts. Finally, in the 4D spectrum, each cross peak is characterized by four chemical-shift coordinates, the proton-chemical shifts of the two protons involved and the chemical shifts of the heavy atoms to which they are attached. Reproduced from Ref. 1.

constants (which are related to ϕ and χ_1, respectively) and the intraresidue and sequential interresidue NOEs involving the NH, C$^\alpha$H and C$^\beta$H protons[29,30]. This information can be supplemented, and often supplanted, by the measurement of heteronuclear couplings by quantitative *J*-correlation spectroscopy. The most useful couplings in this regard are the $^3J_{C\gamma CO}$ and $^3J_{NC\gamma}$ coupling, which provide information on the C–C$_\alpha$–C$_\beta$–C$_\gamma$ and N–C$_\alpha$–C$_\beta$–C$_\gamma$ torsion angles and are sufficient, when used in combination, to derive the appropriate χ_1 sidechain rotamer. A summary of the heteronuclear quantitative *J*-correlation experiments that we currently employ is provided in Table 2.

Assignment of through-space proton–proton interactions within a protein

Although the panoply of 3D heteronuclear experiments is sufficient for the purposes of spectral assignment, further increases in resolution are required for the reliable identification of NOE through-space interactions. This can be achieved by extending the dimensionality still further to four dimensions[31,32] (Fig. 6). Consider a simple 2D spectrum demonstrating 11 cross peaks from aliphatic resonances to a single proton-resonance position. In the 2D spectrum it is impossible to ascertain whether this destination resonance involves one proton or many. Extending the spectrum to 3D by separating the NOE interactions according to the chemical shift of the heavy atom (^{15}N or ^{13}C) attached to each proton reveals that there are three individual protons involved. The identity of the originating aliphatic protons, however, is only specified by their proton-chemical shifts. As the extent of spectral overlap in the aliphatic region of the spectrum is considerable, additional editing is necessary; this is achieved by adding a further dimension, such that each plane of the 3D spectrum now constitutes a cube in the 4D spectrum edited by the ^{13}C shift of the carbon atom attached to each of the originating protons. In this manner, each ^{1}H–^{1}H NOE interaction is specified by four chemical-shift coordinates, the two protons giving rise to the NOE and the heavy atoms to which they are attached.

Because the number of NOE interactions present in each 2D plane of a 4D ^{13}C–^{15}N- or ^{13}C–^{13}C-separated NOE spectrum is so small, the inherent resolution in a 4D spectrum is extremely high, despite the low level of digitization[1]. Furthermore, it can be calculated that 4D spectra with virtual lack of resonance overlap and good sensitivity can be obtained on proteins with as many as 400 residues. Thus, once complete ^{1}H, ^{15}N and ^{13}C assignments are obtained, analysis of 4D ^{13}C–^{15}N- and ^{13}C–^{13}C-separated NOE spectra should permit the assignment of almost all NOE interactions in a relatively straightforward manner[1]. The first successful application of these methods to the structural determination of a protein greater than 15 kDa was achieved in 1991, with the determination of the solution structure of interleukin-1β, a protein of 17 kDa and 153 residues[33]. This has now been extended to a 30 kDa, 259 residue protein, EIN[6] (Fig. 7).
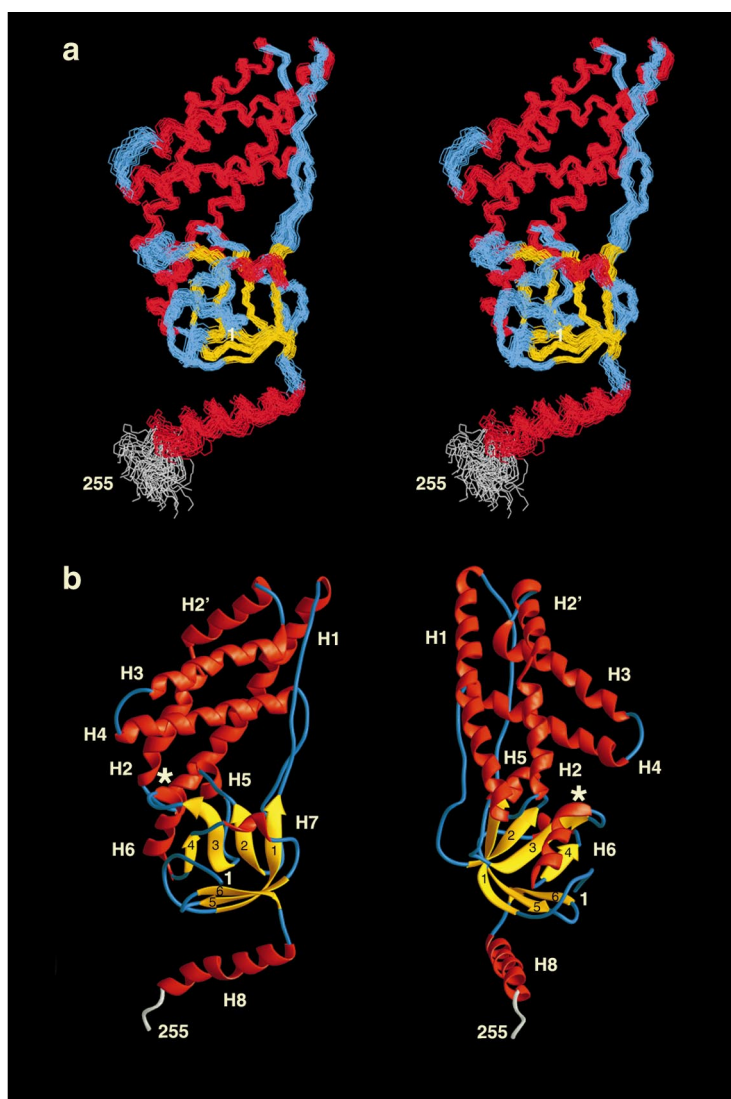
Figure 7
(**a**) Stereoview showing a superposition of the backbone (N, Cα, C) atoms of 50 simulated-annealing structures of the N-terminal domain of Enzyme I (EIN). (**b**) Ribbon diagrams illustrating two views of the backbone of EIN. Helices are shown in red, strands in yellow, loops in blue, and the disordered C-terminus in white. The asterisks indicate the location of the active-site histidine (His189). Reproduced from Ref. 6.

Protein–ligand and protein–protein complexes

If one of the partners in a complex (e.g. a peptide, an oligonucleotide or a drug) presents a relatively simple spectrum that can be assigned by 2D methods, the most convenient strategy for dealing with protein complexes is one in which the protein is labelled with ^{15}N and ^{13}C and the partner is unlabelled (i.e. is at natural isotopic abundance). It is then possible to use a combination of heteronuclear filtering and editing to design experiments in which correlations involving only protein resonances, only ligand resonances or only through-space interactions between ligand and protein are observed[34]. These experiments are summarized in Table 3, and have been successfully employed in a number of laboratories to solve the structures of a number of protein–drug, protein–peptide and protein–DNA complexes (Table 4). It

reviews

should be noted that, to be successful, these experiments require the complexes to be in either slow or fast exchange on the chemical-shift time scale (defined as $k_{diss} \ll 2\pi\Delta\delta$ or $\gg 2\pi\Delta\delta$, respectively, where k_{diss} is the dissociation rate constant and $\Delta\delta$ are the observed differences in chemical shifts between the resonances of the free and complexed forms). If exchange between the free and bound states is intermediate on the chemical-shift time scale ($k_{diss} \approx 2\pi\Delta\delta$), the resonances will be severely broadened.

Homo-oligomeric proteins represent complexes between identical subunits. The first dimer to be solved by NMR was the chemokine interleukin 8 (Ref. 35). Since that time, the structures of a number of other homodimeric systems have been solved (Table 4). More recently, the methodology has been extended to a tetramer, the oligomerization domain of the tumour suppressor p53 (Refs 36–39), and a 44 kDa trimer, the ectodomain of SIV gp41 (Ref. 40). For multimeric proteins, additional labelling schemes can also be used to facilitate the identification of intermolecular NOEs. For example, one subunit can be labelled with ^{15}N and ^2H, the other with ^{13}C and ^1H, enabling high-sensitivity 3D and 4D experiments to be recorded in which NOEs are only observed between protons attached to ^{15}N in one subunit and ^{13}C in the other[40] (Table 3).

Additional methods of structure refinement

The NOE-derived interproton distance and torsion-angle restraints that are traditionally employed in NMR structure determination can be supplemented by direct refinement against a number of other NMR observables in a relatively straightforward manner. These include: three-bond coupling constants[8], which are related to torsion angles; ^{13}C secondary chemical shifts[9], which are related to backbone ϕ and Ψ angles; and ^1H chemical shifts[10,41], which are influenced by short-range ring-current effects from aromatic groups, magnetic anisotropy of C=O and C–N bonds, and electrical-field effects arising from charged groups. The rationale behind including these restraints is twofold: (1) they are easily measured and therefore represent a useful source of additional structural restraints;

Table 3. Summary of heteronuclear nuclear Overhauser enhancement experiments used to study protein–ligand complexes (including protein–nucleic-acid and protein–protein complexes)[1,18,19,34]

Experiment	Nuclear-Overhauser-enhancement connectivity
U–^{15}N–^{13}C protein + U–^{14}N–^{12}C ligand	
Intra- and intermolecular contacts	
3D ^{15}N-separated NOE in H_2O	$H(y)$–$^{15}N(y)$————$H(x)$
3D ^{13}C-separated NOE in D_2O	$H(y)$–$^{13}C(y)$————$H(x)$
Intramolecular protein contacts	
4D ^{13}C–^{13}C-separated NOE in D_2O	$H(y)$–$^{13}C(y)$————$H(x)$–$^{13}C(x)$
4D ^{15}N–^{13}C-separated NOE in H_2O	$H(y)$–$^{15}N(y)$————$H(x)$–$^{13}C(x)$
3D ^{15}N–^{15}N-separated NOE in H_2O	$H(y)$–$^{15}N(y)$————$H(x)$–$^{15}N(x)$
Intramolecular ligand contacts	
2D $^{12}C,^{14}N(F_1)$–$^{12}C,^{14}N(F_2)$ filtered NOE in H_2O	$H(y)$–$^{12}C(y)$————$H(x)$–$^{12}C(x)$
	$H(y)$–$^{14}N(y)$————$H(x)$–$^{12}C(x)$
	$H(y)$–$^{12}C(y)$————$H(x)$–$^{14}N(x)$
	$H(y)$–$^{14}N(y)$————$H(x)$–$^{14}N(x)$
2D $^{12}C(F_1)$–$^{12}C(F_2)$ filtered NOE in D_2O[a]	$H(y)$–$^{12}C(y)$————$H(x)$–$^{12}C(x)$
Intermolecular protein–ligand contacts	
3D ^{15}N-separated(F_2)–$^{14}N,^{12}C(F_3)$ filtered NOE in H_2O	$H(y)$–$^{15}N(y)$————$H(x)$–$^{12}C(x)$
	$H(y)$–$^{15}N(y)$————$H(x)$–$^{14}N(x)$
3D ^{13}C-separated(F_2)–$^{12}C(F_3)$ filtered NOE in D_2O	$H(y)$–$^{13}C(y)$————$H(x)$–$^{12}C(x)$
U–^{15}N–^2H (protein or ligand) + U–^{13}C–^1H (protein or ligand)[b]	
Intramolecular	
3D ^{15}N–^{15}N-separated NOE in H_2O	$H(y)$–$^{15}N(y)$————$H(x)$–$^{15}N(x)$
4D ^{13}C–^{13}C-separated NOE in D_2O	$H(y)$–$^{13}C(y)$————$H_{(}(x)$–$^{13}C(x)$
4D ^{15}N–^{15}N-separated NOE in H_2O	$H(y)$–$^{15}N(y)$————$H(x)$–$^{15}N(x)$
Intermolecular	
3D ^{13}C-separated–^{15}N-filtered	$H(y)$–$^{13}C(y)$————$H(x)$–$^{15}N(x)$
3D ^{15}N-separated–^{13}C-filtered	$H(y)$–$^{15}N(y)$————$H(x)$–$^{13}C(x)_)$
4D ^{13}C-separated–^{15}N-separated	$H(y)$–$^{13}C(y)$————$H(x)$–$^{15}N(x)$

[a]Similar heteronuclear-filtered 2D correlation and Hartmann–Hahn spectra can also be recorded to assign the spin systems of the ligand.

[b]For homomultimeric systems, the multimer needs to be reconstituted from an equimixture of uniformly ^{15}N–^{13}C and ^{14}N–^{12}C, or ^{15}N–^2H and ^{13}C–^1H labelled subunits.

Symbols x and y indicate different residues on the polypeptide chain. F_n represents the different radio frequencies used during multidimensional experiments.

---

reviews

and (2) it is generally found that the agreement between observed and calculated values for these various parameters is better for high-resolution X-ray structures than for the corresponding high-resolution NMR structures refined in the absence of these restraints. The inclusion of these restraints has little impact on the precision (that is, how close the calculated structures are to each other, which is measured by the average atomic root-mean-square deviation of the structures in a given ensemble from the overall mean coordinate positions for the ensemble) but does increase the accuracy (that is, how close the calculated structures are to the 'true' mean structure) of the structures.

Further improvements in the quality of structures generated from NMR data can be obtained by using a conformational database potential representing statistical distributions of dihedral angle relationships in databases of high-resolution, highly refined protein and nucleic-acid crystal structures[11,12]. The rationale for this procedure is based on the observation that uncertainties in the description of the nonbonded contacts represent a key limiting factor in the attainable accuracy of protein NMR structures, and that the nonbonded interaction terms currently used have poor discriminatory power between high- and low-probability local conformations. The idea behind the conformational database potential is to bias sampling during simulated-annealing refinement to conformations that are likely to be energetically feasible by effectively limiting the choices of dihedral angles to those that are known to be physically possible. In this manner, the variability in the structures produced by this method is primarily a function of the experimental restraints, rather than an artefact of a poor nonbonded-interaction model. This can be readily achieved without compromising the agreement with the experimental restraints and the deviations from idealized covalent geometry, which remain within experimental error.

Long-range structural restraints

Until very recently, structural determination by NMR relied exclusively on restraints whose information is entirely local and restricted to atoms close in space, specifically, NOE-derived short (<5 Å) interproton-distance restraints, which may be supplemented by coupling constants, ^{13}C secondary shifts and ^1H shifts. The success of these methods arises from the fact that short interproton distances between units far apart in a linear array are highly conformationally restrictive[1]. However, there are numerous cases where restraints that define long-range order can supply invaluable structural information. In particular, they permit the relative positioning of structural elements that do not have many short-interproton-distance contacts between them. Examples of such situations include modular and multidomain proteins and linear nucleic acids. Two novel approaches have recently been introduced that directly provide restraints that characterize long-range order *a priori*.

Table 4. Protein–drug, protein–peptide and protein–DNA complexes, and homodimeric proteins whose three-dimensional structures have been solved by nuclear magnetic resonance spectroscopy

Complex	Refs
Protein–drug	
Cyclophilin–cyclosporin	47,48
FK506-binding-protein–ascomycin	49
Protein–peptide	
Calmodulin–MLCK-peptide	50
SH2–peptide	51,52
SH3–peptide	53–57
Glutaredoxin–glutathione	58
Human-thioredoxin–NFκB-peptide	59
Human-thioredoxin–Ref1-peptide	60
Protein–DNA	
GATA-1	61
Lac-repressor headpiece	62
Antenennapedia homeodomain	63
DNA-binding domain of c-myb	64
Trp repressor	65
Male-sex-determining factor SRY	66
LEF-1	67
Chromatin remodelling factor GAGA	68
HMG-I(Y)	69
Homodimeric proteins	
Interleukin 8	35
Arc repressor	70
Gene-5 protein from M13	71
Human macrophage inflammatory protein 1β	72
GRO–MGSA	73,74
RANTES	75
Mnt repressor	76
C-terminal domain of HIV-1 integrase	77
C-terminal domain of HIV-2 integrase	78
N-terminal domain of HIV-1 integrase	79

The first relies on the dependence of heteronuclear (^{15}N or ^{13}C) longitudinal (T_1) and transverse (T_2) relaxation times (specifically, T_1/T_2 ratios) on rotational-diffusion anisotropy[13], and the second on residual dipolar couplings in magnetically oriented macromolecules[14]. The two methods provide restraints that are related in a simple geometric manner to the orientation of N–H and C–H internuclear vectors relative to the diffusion and molecular magnetic susceptibility tensors, respectively.

For the heteronuclear ^{15}N T_1/T_2 method to be applicable, the molecule must tumble anisotropically (i.e. it must be nonspherical). The minimum ratio of the diffusion anisotropy for which heteronuclear T_1/T_2 refinement will be useful depends entirely on the accuracy and uncertainties in the measured T_1/T_2 ratios. In practice, the difference between the maximum and minimum observed T_1/T_2 ratio must exceed the uncertainty in the measured T_1/T_2 values by an order of magnitude. This typically means that the diffusion anisotropy should be greater than ~1.5.

Similarly, the applicability of the residual–dipolar–coupling method depends on the magnitude of the magnetic susceptibility anisotropy (that is, the degree of alignment of the molecule in the magnetic field).
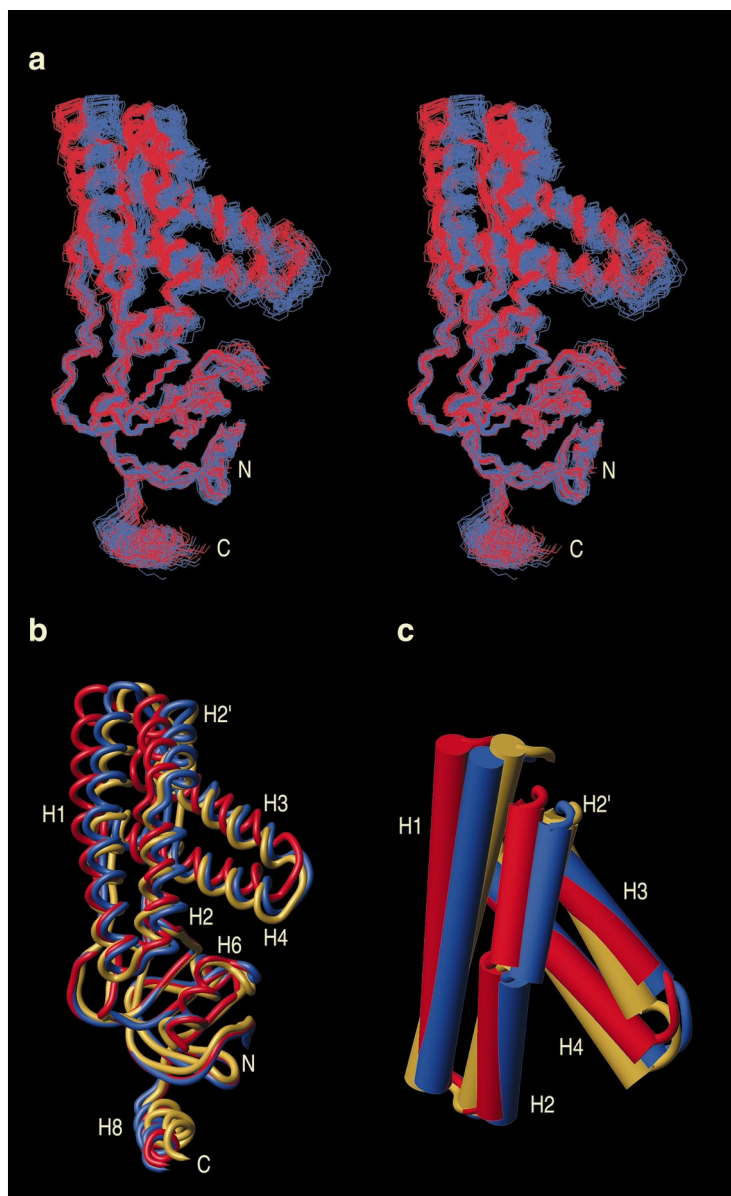
Figure 8

(**a**) Best-fit superposition of the backbone (N, Cα, C) atoms of the ensemble of simu-lated-annealing structures (30 each) of the N-terminal domain of Enzyme I calculated with (red) and without (blue) ^{15}N T_1/T_2 refinement, best-fitted to the α/β domain (residues 2–20 and 148–230). (**b**) and (**c**) Views showing superpositions, best-fitted to the α/β domain, of the restrained, regularized mean structures derived from the ensembles calculated with (red) and without (blue) ^{15}N T_1/T_2 refinement, and of the X-ray structure (yellow). In (**b**), the backbone of residues 1–249 is displayed as a tubular representation; in (**c**) the helices of the α domain are shown as cylinders. Reproduced from Ref. 13.

The magnetic susceptibility of most diamagnetic pro-teins is dominated by aromatic residues, but also con-tains contributions from the susceptibility anisotropies of the peptide bonds. As the magnetic-susceptibility-anistropy tensors of these individual contributors are generally not colinear, the net value of the magnetic susceptibility anisotropy in diamagnetic proteins is usually small. Much larger magnetic susceptibility anisotropies are obtained if many aromatic groups are stacked upon each other in such a way that their mag-netic-susceptibility contributions are additive, as in the case of nucleic acids. Hence, this particular method is ideally suited to protein–nucleic-acid complexes. In practice, the residual dipolar couplings must exceed the uncertainty in their measured values by an order of magnitude, which typically means that the mag-netic susceptibility anisotropy should be approxi-mately -10×10^{-34} m^3 molecule^{-1}, which is about ten times greater than that for benzene. In addition, other methods of alignment can potentially be employed. These include the exploitation of a protein's aniso-tropic-electrical-polarizability and optical-absorption tensors to obtain considerable degrees of alignment by means of strong low-frequency electric fields and polarized light, respectively. The addition of dilute liquid crystals that orient in a magnetic field, such as bicelles, can also be used to obtain considerable degrees of alignment.

An application of direct refinement against ^{15}N T_1/T_2 ratios is illustrated in Figs 8 and 9 for the pro-tein EIN[13]. EIN is elongated in shape, with a diffu-sion anisotropy of ~2. As a result, the observed T_1/T_2 ratios range from ~14 (when the N–H vector is per-pendicular to the diffusion axis) to ~30 (when the N–H vector is parallel to the diffusion axis) (Fig. 9). EIN consists of two domains, and, of the 2818 NOEs used to determine its structure, only 38 involved inter-domain contacts. Refinement against the T_1/T_2 ratios results in a small change in the relative orientations of the two domains (Fig. 8). This is best described in terms of the average angular difference between equivalent helices of the α-domain when best-fitting the structures to the backbone of the α/β domain. This angular difference is 5–7° between the NMR structures refined with and without T_1/T_2 ratios, the same between the NMR structure refined without T_1/T_2 ratios and the X-ray structure, and ~10° between the the NMR structure refined with T_1/T_2 ratios and the X-ray structure.

Perspectives and concluding remarks

The recent development of a whole range of highly sensitive multidimensional heteronuclear edited and filtered NMR experiments has revolutionized the field of protein-structure determination by NMR. Proteins and protein complexes in the 20–50 kDa range are now amenable to detailed structural analysis in solution.

Despite these advances, it should always be borne in mind that there are a number of key requirements that have to be satisfied to permit the successful determi-nation of the structures of larger proteins and protein complexes by NMR: the protein in hand must be sol-uble and should not aggregate up to concentrations of about 0.5–1 mM; it must be stable at room tempera-ture or slightly higher for considerable periods of time (especially as it may take several months of measure-ment time to acquire all the necessary NMR data); it should not exhibit significant conformational hetero-geneity, which could result in extensive line broaden-ing; and, finally, it must be amenable to uniform ^{15}N and ^{13}C labelling. At the present time, there are
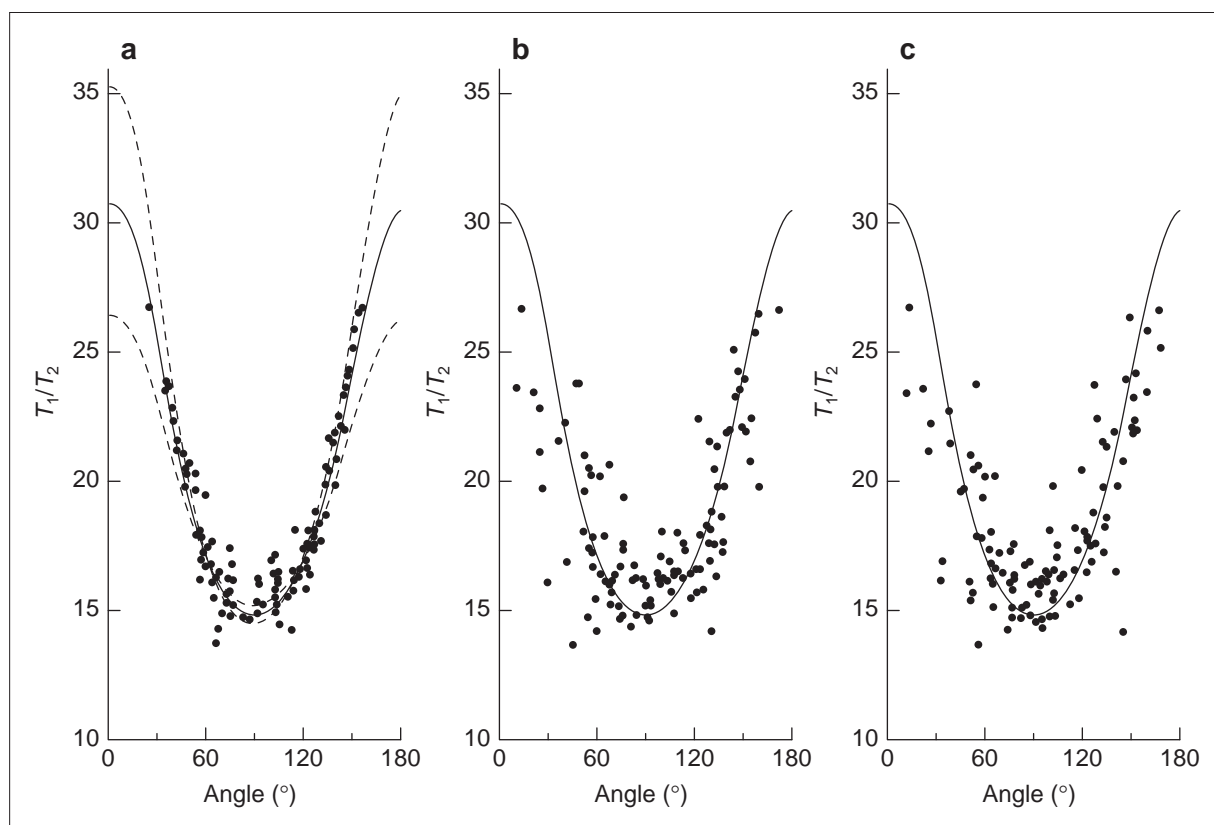
Figure 9

Dependence of the observed ^{15}N T_1/T_2 ratios at 600 MHz on the angle θ between the NH-bond vectors and the unique axis of the diffusion tensor for the restrained, regularized mean structures of the N-terminal domain of Enzyme I obtained from the ensembles calculated with (**a**) and without (**b**) ^{15}N T_1/T_2 refinement, and for the X-ray structure (**c**). The solid lines represent the theoretical dependence of T_1/T_2 on θ for a diffusion anisotropy of 2.1 and an effective correlation time of 13.1 ns. The dashed lines in (**a**) illustrate the effects on the theoretical dependence of T_1/T_2 on θ of increasing or decreasing the diffusion anisotropy by 15%. Reproduced from Ref. 13.

relatively few examples in the literature of proteins in the 15–30 kDa range that have had their structures solved by NMR. Likewise, the structures of only a handful of protein complexes (with DNA or peptides) and oligomers have been determined to date using these methods. It can be anticipated, however, that over the next few years, by the widespread use of multidimensional heteronuclear NMR experiments coupled with semiautomated assignment procedures, many more NMR structures of proteins and protein complexes will become available.

References

1 Clore, G. M. and Gronenborn, A. M. (1991) *Science* 252, 1390–1399
2 Wüthrich, K. (1986) *NMR of Proteins and Nucleic Acids*, Wiley
3 Clore, G. M. and Gronenborn, A. M. (1987) *Protein Eng.* 1, 275–288
4 Dyson, H. J., Gippert, G. P., Case, D. A., Holmgren, A. and Wright, P. E. (1990) *Biochemistry* 29, 4129–4136
5 Forman-Kay, J. D., Clore, G. M., Wingfield, P. T. and Gronenborn, A. M. (1991) *Biochemistry* 30, 2685–2698
6 Garrett, D. S., Seok, Y-J., Liao, D-I., Peterkofksy, A., Gronenborn, A. M. and Clore, G. M. (1997) *Biochemistry* 36, 2517–2530
7 Martin, J. R. *et al.* (1997) *Structure* 5, 521–532
8 Garrett, D. S. *et al.* (1994) *J. Magn. Reson. Ser. B* 104, 99–103
9 Kuszewski, J., Qin, J., Gronenborn, A. M. and Clore, G. M. (1995) *J. Magn. Reson. Ser. B* 106, 92–96
10 Kuszewski, J., Gronenborn, A. M. and Clore, G. M. (1995) *J. Magn. Reson. Ser. B* 107, 293–297
11 Kuszewski, J., Gronenborn, A. M. and Clore, G. M. (1996) *Protein Sci.* 5, 1067–1080
12 Kuszewski, J., Gronenborn, A. M. and Clore, G. M. (1997) *J. Magn. Reson.* 125, 171–177
13 Tjandra, N., Garrett, D. S., Gronenborn, A. M., Bax, A. and Clore, G. M. (1997) *Nat. Struct. Biol.* 4, 443–449
14 Tjandra, N., Omichinski, J. G., Gronenborn, A. M., Clore, G. M. and Bax, A. (1997) *Nat. Struct. Biol.* 4, 732–738
15 Ernst, R. R., Bodenhausen, G. and Wokaun, A. (1987) *Principles of Nuclear Magnetic Resonance in One and Two Dimensions*, Clarendon Press
16 Oschkinat, H. *et al.* (1988) *Nature* 332, 374–376
17 Clore, G. M. and Gronenborn, A. M. (1989) *Crit. Rev. Biochem. Mol. Biol.* 24, 479–564
18 Clore, G. M. and Gronenborn, A. M. (1991) *Progr. Nucl. Magn. Reson. Spectrosc.* 23, 43–92
19 Bax, A. and Grzesiek, S. (1993) *Acc. Chem. Res.* 26, 131–138
20 Grzesiek, S., Wingfield, P. T., Stahl, S. J. and Bax, A. (1995) *J. Am. Chem. Soc.* 117, 9594–9595
21 Venters, R. A., Metzler, W. J., Spicer, L. D., Mueller, L. and Farmer, B. T., II (1995) *J. Am. Chem. Soc.* 117, 9592–9593

reviews

22 Vuister, G. W., Kim, S-J., Wu, C. and Bax, A. (1994) *J. Am. Chem. Soc.* 116, 9206–9210
23 Driscoll, P. C., Clore, G. M., Marion, D., Wingfield, P. T. and Gronenborn, A. M. (1990) *Biochemistry* 29, 3542–3556
24 Bax, A. and Pochapsky, S. S. (1992) *J. Magn. Reson.* 99, 638–643
25 Kay, L. E., Keifer, P. and Saarinen, T. (1992) *J. Am. Chem. Soc.* 114, 10 663–10 665
26 Griesinger, C., Sørensen, O. W. and Ernst, R. R. (1986) *J. Chem. Phys.* 85, 6837–6852
27 Bax, A. *et al.* (1994) *Methods Enzymol.* 239, 79–105
28 Wagner, G., Braun, W., Havel, T. F., Schaumann, T., Go, N. and Wüthrich, K. (1987) *J. Mol. Biol.* 196, 611–639
29 Güntert, P., Braun, W., Billeter, M. and Wüthrich, K. (1989) *J. Am. Chem. Soc.* 111, 3397–4004
30 Nilges, M., Clore, G. M. and Gronenborn, A. M. (1990) *Biopolymers* 29, 813–822
31 Kay, L. E., Clore, G. M., Bax, A. and Gronenborn, A. M. (1991) *Science* 249, 411–414
32 Clore, G. M., Kay, L. E., Bax, A. and Gronenborn, A. M. (1991) *Biochemistry* 30, 12–18
33 Clore, G. M., Wingfield, P. T. and Gronenborn, A. M. (1991) *Biochemistry* 30, 2315–2323
34 Kuszewski, J., Gronenborn, A. M. and Clore, G. M. (1996) *J. Magn. Reson. Ser. B* 112, 79–81
34 Gronenborn, A. M. and Clore, G. M. (1995) *Crit. Rev. Biochem. Mol. Biol.* 30, 351–385
35 Clore, G. M., Appella, E., Yamada, M., Matsushima, K. and Gronenborn, A. M. (1990) *Biochemistry* 29, 1689–1696
36 Clore, G. M. *et al.* (1994) *Science* 265, 386–391
37 Clore, G. M. *et al.* (1995) *Science* 267, 1515–1516
38 Clore, G. M. *et al.* (1995) *Nat. Struct. Biol.* 2, 321–332
39 Lee, W. *et al.* (1994) *Nat. Struct. Biol.* 1, 877–890
40 Caffrey, M. *et al.* (1997) *J. Mol. Biol.* 271, 819–826
41 Kuszewski, J., Gronenborn, A. M. and Clore, G. M. (1996) *J. Magn. Reson. Ser. B* 112, 79–81
42 Grzesiek, S. and Bax, A. (1997) *J. Biomol. NMR* 9, 207–211
43 Hu, J-S. and Bax, A. (1997) *J. Am. Chem. Soc.* 119, 6360–6368
44 Grzesiek, S., Kuboniwa, H., Hinck, A. P. and Bax, A. (1995) *J. Am. Chem. Soc.* 117, 5312–5315
45 Hu, J-S., Grzesiek, S. and Bax, A. (1997) *J. Am. Chem. Soc.* 119, 1803–1804
46 Hu, J-S. and Bax, A. *J. Biomol. NMR* (in press)
47 Theriault, Y. *et al.* (1993) *Nature* 361, 88–91
48 Spitzfaden, C., Braun, W., Wider, G., Widmer, H. and Wüthrich, K. (1994) *J. Biomol. NMR* 4, 463–482
49 Meadows, R. P. *et al.* (1993) *Biochemistry* 32, 754–765
50 Ikura, M., Clore, G. M., Gronenborn, A. M., Zhu, G., Klee, C. B. and Bax, A. (1992) *Science* 256, 632–638
51 Pascal, S. M. *et al.* (1994) *Cell* 77, 461–472
52 Xu, R. X., Word, J. M., David, D. G., Rink, M. J., Willard, D. H. and Gampe, R. T. (1995) *Biochemistry* 34, 2107–2121
53 Wittekind, M. *et al.* (1994) *Biochemistry* 33, 13 531–13 539
54 Terasawa, H. *et al.* (1994) *Nat. Struct. Biol.* 1, 891–897
55 Goudreau, N., Cornille, F., Duchesne, M., Tocque, B., Garbay, C. and Roques, B. P. (1994) *Nat. Struct. Biol.* 1, 898–907
56 Yu, H., Chen, J. K., Feng, S., Dalgarno, D. C., Brauer, A. W. and Schreiber, S. L. (1994) *Cell* 76, 933–945
57 Feng, S., Chen, J. K., Yu, H., Simon, J. A. and Schreiber, S. L. (1994) *Science* 266, 1241–1245
58 Bushweller, J. H., Billeter, M., Holmgren, A. and Wüthrich, K. (1994) *J. Mol. Biol.* 235, 1585–1597
59 Qin, J., Clore, G. M., Kennedy, W. M. P., Huth, J. R. and Gronenborn, A. M. (1995) *Structure* 3, 289–297
60 Qin, J., Clore, G. M., Kennedy, W. P., Kuszewski, J. and Gronenborn, A. M. (1996) *Structure* 4, 613–620
61 Omichinski, J. G. *et al.* (1993) *Science* 261, 438–446
62 Chuprina, V. P., Rullman, J. A. C., Lamerichs, R. M. N. J., van Boom, J. H., Boelens, R. and Kaptein, R. (1993) *J. Mol. Biol.* 234, 446–462
63 Billeter, M., Qian, Y. Q., Otting, G., Müller, M., Gehring, W. and Wüthrich, K. (1993) *J. Mol. Biol.* 234, 1084–1097
64 Ogata, K. *et al.* (1994) *Cell* 79, 639–648
65 Zhang, H. *et al.* (1994) *J. Mol. Biol.* 238, 592–614
66 Werner, M. H., Huth, J. R., Gronenborn, A. M. and Clore, G. M. (1995) *Cell* 81, 705–714
67 Love, J. J., Li, X., Case, D. A., Giese, K., Grosschedl, R. and Wright, P. E. (1995) *Nature* 376, 791–795
68 Omichinski, J. G., Pedone, P. V., Felsenfeld, G., Gronenborn, A. M. and Clore, G. M. (1997) *Nat. Struct. Biol.* 4, 122–132
69 Huth, J. R. *et al.* (1997) *Nat. Struct. Biol.* 4, 657–665
70 Bonvin, A. M. J. J., Vis, H., Breg, J. N., Burgering, M. J. M., Boelens, R. and Kaptein, R. (1994) *J. Mol. Biol.* 236, 328–341
71 Folkers, P. J. M., Nilges, M., Folmer, R. H. A., Konnings, R. N. H. and Hilbers, C. W. (1994) *J. Mol. Biol.* 236, 229–246
72 Lodi, P. J. *et al.* (1994) *Science* 263, 1762–1767
73 Fairbrother, W. J., Reilly, D., Colby, T. J., Hesselgesser, J. and Horuk, R. (1994) *J. Mol. Biol.* 242, 252–270
74 Kim, K-S., Clark-Lewis, I. and Sykes, B. D. (1994) *J. Biol. Chem.* 269, 32 909–32 915
75 Skelton, N. J., Aspiras, F., Ogez, J. and Scall, T. J. (1995) *Biochemistry* 34, 5329–5342
76 Burgering, M. J. M. *et al.* (1994) *Biochemistry* 33, 15 036–15 045
77 Lodi, P. J. *et al.* (1995) *Biochemistry* 34, 9826–9833
78 Eijkelenboom, A. P. *et al.* (1995) *Nat. Struct. Biol.* 2, 807–810
79 Cai, M., Zheng, R., Caffrey, M., Craigie, R., Clore, G. M. and Gronenborn, A. M. (1997) *Nat. Struct. Biol.* 4, 567–577

**Do you disagree?
Was something missing?
Tell us about it!**

If you have any comments of general interest to biotechnologists or additional recent published information relevant to any articles in *TIBTECH* – let us know.

Letters to the Editor should be concise (maximum 800 words), and addressed to:
Dr Meran Owen (Editor),
Trends in Biotechnology, Elsevier Trends Journals,
68 Hills Road, Cambridge, UK CB2 1LA.

Please mark clearly whether or not the letter is intended for publication.